Molecular Biophysics:

Metal-driven Operation of the Human Large-conductance Voltage- and Ca^{2+} -dependent Potassium Channel (BK) Gating Ring Apparatus

Anoosh D. Javaherian, Taleh Yusifov, Antonios Pantazis, Sarah Franklin, Chris S. Gandhi and Riccardo Olcese

J. Biol. Chem. 2011, 286:20701-20709.
doi: 10.1074/jbc.M111.235234 originally published online April 6, 2011

THE JOURNAL OF BIOLOGICAL CHEMISTRY VOL. 286, NO. 23, pp. 20701–20709, June 10, 2011

Metal-driven Operation of the Human Large-conductance Voltage- and Ca^{2+}-dependent Potassium Channel (BK) Gating Ring Apparatus*[S]◆

Received for publication, February 25, 2011, and in revised form, April 4, 2011 Published, JBC Papers in Press, April 6, 2011, DOI 10.1074/jbc.M111.235234

Anoosh D. Javaherian[‡1], Taleh Yusifov[‡1], Antonios Pantazis[‡2], Sarah Franklin[‡], Chris S. Gandhi[§], and Riccardo Olcese[‡¶‖3]

From the [‡]Division of Molecular Medicine, Department of Anesthesiology, [¶]Cardiovascular Research Laboratory, and [‖]Brain Research Institute, David Geffen School of Medicine, UCLA, Los Angeles, California 90095-7115 and the [§]Division of Chemistry and Chemical Engineering, California Institute of Technology, Pasadena, California 91125

Large-conductance voltage- and Ca^{2+}-dependent K^+ (BK, also known as MaxiK) channels are homo-tetrameric proteins with a broad expression pattern that potently regulate cellular excitability and Ca^{2+} homeostasis. Their activation results from the complex synergy between the transmembrane voltage sensors and a large (>300 kDa) C-terminal, cytoplasmic complex (the "gating ring"), which confers sensitivity to intracellular Ca^{2+} and other ligands. However, the molecular and biophysical operation of the gating ring remains unclear. We have used spectroscopic and particle-scale optical approaches to probe the metal-sensing properties of the human BK gating ring under physiologically relevant conditions. This functional molecular sensor undergoes Ca^{2+}- and Mg^{2+}-dependent conformational changes at physiologically relevant concentrations, detected by time-resolved and steady-state fluorescence spectroscopy. The lack of detectable Ba^{2+}-evoked structural changes defined the metal selectivity of the gating ring. Neutralization of a high-affinity Ca^{2+}-binding site (the "calcium bowl") reduced the Ca^{2+} and abolished the Mg^{2+} dependence of structural rearrangements. In congruence with electrophysiological investigations, these findings provide biochemical evidence that the gating ring possesses an additional high-affinity Ca^{2+}-binding site and that Mg^{2+} can bind to the calcium bowl with less affinity than Ca^{2+}. Dynamic light scattering analysis revealed a reversible Ca^{2+}-dependent decrease of the hydrodynamic radius of the gating ring, consistent with a more compact overall shape. These structural changes, resolved under physiologically relevant conditions, likely represent the molecular transitions that initiate the ligand-induced activation of the human BK channel.

The large-conductance voltage- and Ca^{2+}-activated K^+ channel (BK,[4] MaxiK, Slo1) is an important regulator of cellular function including cellular excitability, neurotransmitter release, vascular tone, and hair cell tuning (1–8). Its K^+ conductance of ~250 picosiemens is an order of magnitude larger than that observed in typical voltage-gated K^+-selective channels (9), making the BK channel a powerful regulator of the cell membrane potential. A functional BK channel is composed of four identical α subunits, each consisting of a short extracellular N-terminal tail, seven transmembrane segments (S0–S6) (10, 11), and a large intracellular C-terminal domain. The four α subunits likely assemble around a central symmetry axis, forming the K^+-selective pore, surrounded by peripheral transmembrane voltage-sensing domains (12, 13) that undergo conformational rearrangements upon membrane depolarization (14–16) to facilitate pore opening (17–20). Another pathway to BK channel activation is mediated by intracellular Ca^{2+}. In the CNS, BK channels localize within Ca^{2+} nanodomains generated at the immediate proximity of voltage-gated Ca^{2+} channels as an efficient strategy to regulate BK channel activity (reviewed by Ref. 21). Intracellular Ca^{2+} sensitivity is conferred by a large "gating ring" tetrameric superstructure, which is composed of two tandem C-terminal regulators of K^+ conductance (RCK1 and RCK2) domains from each of the four channel α subunits (22–24). The gating ring apparatus regulates BK channel activation by micromolar Ca^{2+} and millimolar Mg^{2+} (4, 7, 8, 25) as it is also expected to undergo ligand-driven conformational rearrangements that in turn favor channel opening (26–28). A region containing five consecutive aspartates (Asp^{894}–Asp^{898}) termed the "calcium bowl" (29) constitutes a high-affinity Ca^{2+}-binding site (24, 30–33) located within the RCK2 domain (23, 24, 33). Consistent with evidence that the neutralization of the calcium bowl region reduces, but does not abolish, Ca^{2+} sensitivity, a second high-affinity Ca^{2+}-sensing region is thought to exist within the RCK1 domain, where residues aspartate 367, methionine 513, arginine 514, and glutamate 535 have a critical role in the Ca^{2+} sensitivity of the channel (34–38). The human BK channel mutation D434G (in RCK1), thought to pathologically enhance the Ca^{2+}-sensing

* This work was supported, in whole or in part, by National Institutes of Health Research Grant NIGMS R01GM082289 and the Laubisch Foundation (to R. O.).
◆ This article was selected as a Paper of the Week.
[S] The on-line version of this article (available at http://www.jbc.org) contains supplemental Figs. S1–S4 and Tables S1–S4.
[1] Both authors contributed equally to this work.
[2] Recipient of American Heart Association (Western States Affiliate) Postdoctoral Fellowship 09POST2250648.
[3] To whom correspondence should be addressed: Dept. of Anesthesiology, Division of Molecular Medicine, BH-570 CHS, David Geffen School of Medicine, UCLA, Los Angeles, CA. Tel.: 310-206-2214; Fax: 310-206-1947; E-mail: rolcese@ucla.edu.

[4] The abbreviations used are: BK, large-conductance voltage- and Ca^{2+}-activated K^+ (Slo1) channels; CTD, C-terminal domain; DLS, dynamic light scattering; RCK, regulators of K^+ conductance; λ_{ex}, excitation wavelength; λ_{em}, emission wavelength.

mechanism of the channel (39), has been linked to generalized epilepsy and paroxysmal dyskinesia (40). Low-affinity Mg^{2+} sensing depends on coordinating residues within RCK1 (glutamines 374/399) (34, 41) and the transmembrane voltage sensor domain (aspartate 99, asparagine 172) (4, 7, 42, 43). The gating ring is thought to be the site of action of different cytosolic interacting partners (2, 44) as well as small signaling molecules such as reactive oxygen species, CO, hemin, and H^+ (4, 5, 45, 46).

BK channels have been visualized at 17–20 Å resolution (22) and, more recently, atomic structures (3 Å resolution) of the human BK gating ring have been reported (23, 24). Thus, although the BK gating ring has a well defined structural identity, the functional properties linked to its ligand-sensing operation have not yet been investigated. We have probed the structural and functional properties of the recombinant human BK channel C terminus under physiologically relevant conditions, providing evidence that RCK1-RCK2 complexes assemble into a tetrameric gating ring structure that undergoes metal-dependent conformational rearrangements. The resolved molecular events are likely associated with the ligand-induced signal propagation that activates the channel pore. The gating ring superstructure appears to possess the structural and functional properties of a chemo-mechanical coupler able to transduce the free energy of ligand binding into mechanical work.

EXPERIMENTAL PROCEDURES

Expression and Purification—Expression and mutagenesis corresponding to the wild-type and calcium bowl-neutralized (D894A,D895A,D896A,D897A,D898A) human BK C-terminal domain (^{322}IIE···ALK^{1005}) were performed as described previously (33, 47). Briefly, protein fractions were solubilized in 20 mM Tris-HCl and 8 M urea (pH 8.0). The supernatant obtained after centrifugation was applied to a nickel-nitrilotriacetic acid affinity column, and the protein fractions were eluted with (in mM) 250 imidazole and dialyzed against (in mM) 25 MOPS, 2 EGTA, 120 KCl, pH 7.2. The purity of the expressed proteins was analyzed using a 12.5% SDS-PAGE. Protein concentrations were determined using the Biuret-Lowry assay.

Mass Spectrometry (MS)—Enzyme digestion was performed as follows. Purified human Slo1 was separated by SDS-PAGE and in-gel digested prior to analysis by mass spectrometry. Gel plugs were dehydrated in acetonitrile and dried completely in a SpeedVac. Samples were reduced and alkylated with 10 mM dithiothreitol and 10 mM tris(2-carboxyethyl)phosphine solution in 50 mM NH_4HCO_3 (30 min at 56 °C) and 100 mM iodoacetamide (45 min in dark), respectively. Gel plugs were washed with 50 mM NH_4HCO_3, dehydrated with acetonitrile, and dried down in a SpeedVac. Gel pieces were then swollen in digestion buffer containing 50 mM NH_4HCO_3 and 20.0 ng/μl chymotrypsin (25 °C, overnight).

MS Analyses and Database Searching—10 μl of extracted peptides were analyzed by nanoflow LC/MS/MS on a Thermo Orbitrap with a dedicated Eksigent nanopump using a reversed phase column (75-μm inner diameter, 10-cm BioBasic C18, 5-μm particle size, New Objective). Spectra were acquired in data-dependent mode with dynamic exclusion where the instrument selects for fragmentation the top six most abundant ions in the parent spectra. Data were searched against an *Escherichia coli* database inserted with the human Slo1 BK channel amino acid sequence using the SEQUEST algorithm in the BioWorks software program version 3.3.1 SP1. All spectra used for identification had deltaCN > 0.1 and met the following Xcorr criteria: >2 (+1), >3 (+2), >4 (+3), and >5 (+4). Mass tolerance was 2 Da for precursor and 1 Da for product ions.

Circular Dichroism (CD) Spectroscopy—CD spectra were obtained as described previously (33, 47). Briefly, far-UV spectra of purified gating ring in 20 mM phosphate (pH 7.2) were recorded as an average of 7–9 scans. Secondary structure fractions were calculated using the CONTINLL, SELCON3, and CDSSTR algorithms with the SMP56 reference set of the CDPro software package (48). The numbers of α-helices and β-strands were calculated by dividing the numbers of residues included in the distorted α-helix and β-structure by a factor of four and two, respectively.

Size-exclusion Chromatography—Size-exclusion chromatography experiments were performed as described previously (47). Purified BK gating ring in (in mM) 50 Tris-HCl, 2 β-mercaptoethanol, and 2 EGTA (pH 8.4) or (in mM) 20 MOPS (pH 7.2) was loaded onto a Superdex 200 10/300 column equilibrated with the same buffer with a flow rate of 0.5 ml/min. Calibration was performed using protein standards (Sigma).

Time-resolved Trp Fluorescence Spectroscopy—The time-resolved fluorescence lifetime of intrinsic Trp was measured with a Fluorolog-3 spectrofluorometer (Horiba Jobin Yvon) using time-correlated single photon counting (λ_{ex} = 296 nm, λ_{em} = 340 nm) in (in mM) 25 MOPS, 120 KCl, 2 EGTA, pH 7.2. Free ion concentrations were estimated using WEBMAXC or measured as described previously (47).

The instrument response function was acquired using a non-fluorescent, light scattering sample (Ludox, colloidal silica). The instrument response function is a function of the detector characteristics and timing electronics and demonstrates the speed of the instrument and its detection properties. It is the shortest time profile that can be recorded by the instrument (49).

The fluorescence intensity decay data were fit to a sum of three exponential functions, using the DAS6 v6.4 software (Horiba Jobin Yvon)

$$I(t) = \sum_{i=1}^{n} \alpha_i \exp(-t/\tau_i) \quad \text{(Eq. 1)}$$

where I is the fluorescence intensity and α and τ are the normalized pre-exponential factor and decay time constant, respectively. The average fluorescence lifetimes (τ_{avg}) for three-exponential iterative fittings are calculated from the decay times and pre-exponential factors using the equation

$$\tau_{avg} = \sum_{i=1}^{n} f_i \tau_i \quad \text{(Eq. 2)}$$

where f_i is the fractional contribution of each decay time to the steady-state intensity, which is given by

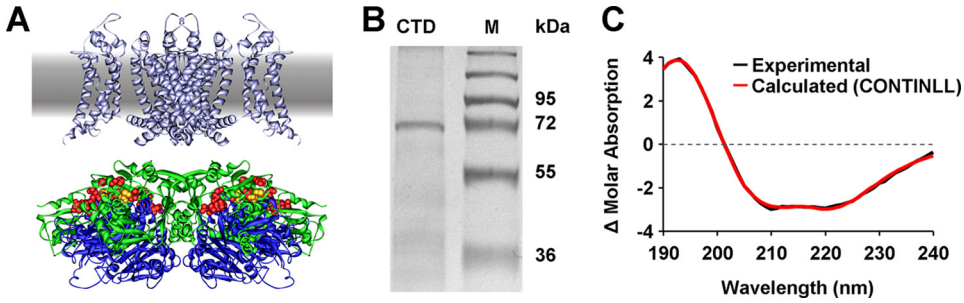

FIGURE 1. **Amino acid sequence, purification, and secondary structure analysis of the recombinant BK CTD.** *A*, BK channel model based on the transmembrane domain of the Kv1.2–2.1 chimera (Protein Data Bank code 2R9R) (18) and the BK gating ring (code 3NAF) (23). The gating ring, formed by four RCK1 (*green*) and four RCK2 (*blue*) domains, assembles below the transmembrane domain. Residues known to be involved in high-affinity Ca^{2+} sensitivity in the BK gating ring are depicted in *red* (Asp^{362}/Asp^{367} in RCK1 and the calcium bowl in RCK2) or *orange* (Met^{513} in RCK1). *B*, SDS-PAGE of the purified CTD shows a single band of estimated molecular mass (*lane M*) of ~72 kDa. *C*, the experimental far-UV CD spectrum of the purified BK CTD is shown as a *black curve*, and the theoretical CONTINLL-calculated curve is shown superimposed in *red*. A change in molar absorption is defined as $\Delta\epsilon\,M^{-1}\,cm^{-1}$. See supplemental Fig. S2*A* for secondary structure parameters.

$$f_i = \alpha_i\tau_i / \sum \alpha_j\tau_j \qquad \text{(Eq. 3)}$$

The goodness of the fit was determined from its χ^2 value and the variance of the weighted residual distribution ($n = 3$, unless otherwise noted).

Steady-state Fluorescence Spectroscopy—Steady-state Trp fluorescence emission spectra of the gating ring in (in mM) 25 MOPS, 120 KCl, 2 EGTA, pH 7.2, were acquired in the 310–400 nm range, $\lambda_{ex} = 295$ nm (5 nm excitation/emission slit width). Normalized fluorescence data were fit with a Hill function in the form

$$F = (F_{max} - F_{min})/(1 + ([M^{2+}])/K_{1/2})^n + F_{min} \qquad \text{(Eq. 4)}$$

where F is the fluorescence intensity at 340 or 350 nm for WT and calcium bowl mutant gating ring, respectively; $[M^{2+}]$ is the concentration of Ca^{2+} or Mg^{2+}; $K_{1/2}$ is the apparent dissociation constant; and n is the Hill coefficient.

Dynamic Light Scattering (DLS)—DLS measurements were recorded using a NICOMP 380 submicron particle sizing system. The hydrodynamic properties of gating ring particles were determined by measuring the translational diffusion coefficient D_T, which is related to the frictional coefficient f by the Einstein-Sutherland equation

$$D_T = K_BT/f(cm^2/s) \qquad \text{(Eq. 5)}$$

where K_B is the Boltzmann constant and T is the temperature in K. The frictional coefficient of a spherical particle, f_{sph}, is a function of the fluid viscosity, η, and the radius of the particle, r_{sph}. It is defined by the Stokes law.

$$f_{sph} = 6\pi\eta r_{sph} \qquad \text{(Eq. 6)}$$

Mean particle size distribution was analyzed in volume-weighted Nicomp-fit mode. The theoretical hydrodynamic radius ($R^{theo}{}_H$) was calculated from the formula

$$R^{theo}{}_H = [(3M(V_s + h))/4\pi N_A]^{1/3} \qquad \text{(Eq. 7)}$$

where M is the molecular mass of the gating ring (312,000), V_s is the particle specific volume (0.73 $cm^3\,g^{-1}$), h is the hydration (0.35 g of H_2O (g-protein)$^{-1}$), and N_A is Avogadro's constant (50).

The Perrin, or shape factor, is the ratio of the measured frictional coefficient f to the frictional coefficient f^{theo} of a hypothetical sphere, where

$$F = f/f^{theo} = R_H/R^{theo}{}_H \qquad \text{(Eq. 8)}$$

The polydispersity (P_d) was evaluated according to the following equation

$$P_d = \sigma/D_H \cdot 100\% \qquad \text{(Eq. 9)}$$

where σ is the standard deviation of the distribution and D_H is the mean hydrodynamic diameter from DLS measurements.

RESULTS

Structural Organization of the BK Gating Ring in Solution—The intracellular C-terminal domain (CTD, 684 amino acids) of the BK channel, which accounts for >60% of the whole channel and includes the two ligand-sensing modules RCK1 and RCK2 (supplemental Fig. S1), was expressed and purified. The CTD electrophoretic mobility in SDS-PAGE corresponds to an estimated $M_r = 72{,}000$ (Fig. 1*B*), close to the theoretical molecular weight of the purified protein (78,000). The identity of the purified BK CTD was confirmed by mass spectrometry, which identified 67% of the primary sequence (supplemental Fig. S1). The secondary and quaternary structures of the protein were investigated under physiologically relevant ionic conditions similar to the intracellular environment to ascertain its proper folding and native assembly, information necessary for the validity of the results of subsequent functional assays.

CD spectra were acquired to probe the secondary structure composition of the CTD in solution (Fig. 1*C*) and were subsequently analyzed using algorithms of the CDPro software (48). The experimental (*black*) and calculated (*red*, CONTINLL algorithm) spectra are shown superimposed. The CD spectral analysis revealed a CTD secondary structure composition of ~29% α-helix, ~22% β-strand, organized in 22 α-helices and 30 β-strands, and ~49% turn and unordered structure (supplemental Fig. S2*A*). Although a direct comparison of secondary structure composition across a crystal structure study is not straightforward because of differences in the regions purified and/or resolved, reasonable correlation exists (supplemental Fig. S2).

The oligomeric state of the BK CTD was assessed by size-exclusion chromatography. A characteristic column elution and corresponding calibration curve is shown in Fig. 2, *A* and *B*,

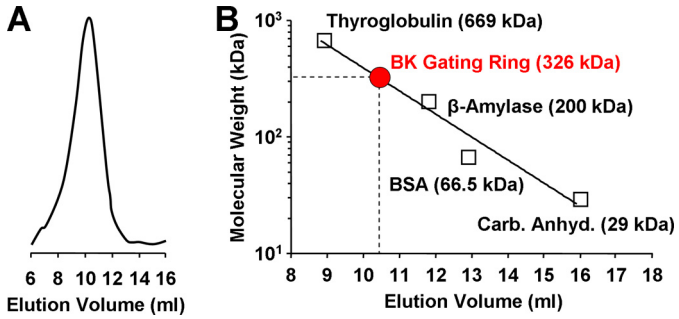

FIGURE 2. **BK C termini assemble into tetramers in solution.** *A*, representative elution profile of BK CTD from a Superdex 200 10/300 column. The peak (at 10.3 ml) corresponds to M_r = 326,000, as estimated from the calibration curve constructed with proteins of known molecular mass (thyroglobulin, β-amylase, bovine serum albumin, and carbonic anhydrase (*Carb. Anhyd.*)), shown in *B*. The mean molecular weight estimated from 15 column elutions was 324,000 ± 4,000. As a theoretical CTD tetramer would have M_r = 78,000 × 4 = 312,000, these data support the view that in solution, the purified CTD forms tetrameric structures, likely corresponding to the BK gating ring.

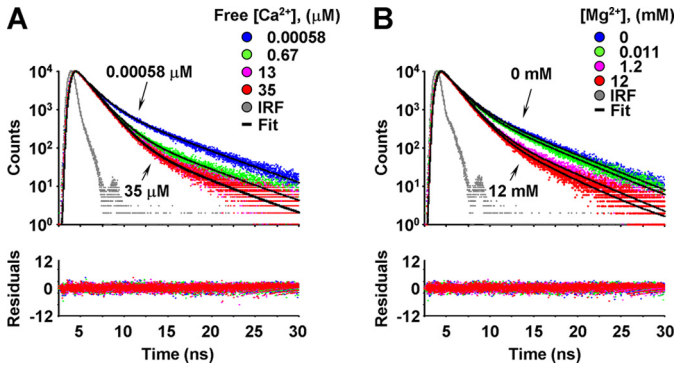

FIGURE 3. **Ca^{2+} and Mg^{2+} induce conformational changes in the BK gating ring.** *A* and *B* show superimposed time-resolved fluorescence intensity decays of the gating ring native Trp residues recorded in increasing [Ca^{2+}] and [Mg^{2+}], respectively. The intrinsic Trp fluorescence emission was measured at 340 nm (λ_{ex} = 296 nm). The fluorescence lifetime is progressively reduced by the addition of micromolar free Ca^{2+} or millimolar Mg^{2+}, suggesting cation-induced conformational change(s). The instrument response time (*IRF*) is shown in *gray*. Fitting parameters for the Ca^{2+} and Mg^{2+} experiments are in supplemental Tables S1 and S2, respectively.

respectively. The BK CTD eluted with an M_r = 324,000 ± 4,000, which is approximately four times the estimated molecular weight of the monomer (78,000), suggesting that in solution, the BK CTDs (RCK1-RCK2 complexes without transmembrane structures) self-assemble into tetramers, likely corresponding to the BK gating ring apparatus.

Ca^{2+} and Mg^{2+} Induce Conformational Changes in the BK Gating Ring—As a chemo-mechanical signal transducer, the gating ring is expected to regulate BK channel open probability by converting the free energy of ligand binding into conformational rearrangements that facilitate channel opening (5, 25, 26, 28, 51–53).

The purified gating ring includes five Trp residues per subunit that serve as intrinsic environment-sensitive fluorophores reporting ligand-induced structural changes (49). We probed the gating ring for metal-induced conformational rearrangements by measuring the fluorescence lifetime of gating ring Trp residues (λ_{ex} = 296 nm; λ_{em} = 340 nm) in solutions with different [Ca^{2+}] or [Mg^{2+}], using time-correlated single-photon counting (49). Fig. 3 shows superimposed data obtained at four different concentrations of Ca^{2+} (Fig. 3*A*) or Mg^{2+} (Fig. 3*B*), represented as single photon detection events binned by the time interval of detection after the excitation pulse; shorter Trp fluorescence lifetimes will result in fewer photons detected at long time intervals, accelerating the decay of the photon histogram. Each photon histogram was fit by the sum of three exponentials (*black curves*) to determine the mean fluorescence lifetime (τ_{avg}) of the native gating ring Trp residues, under different [Ca^{2+}] or [Mg^{2+}].

The average fluorescence lifetime (τ_{avg}) of the gating ring in nominal zero Ca^{2+} (0.00058 μM) was 2.6 ± 0.010 ns. Increasing free [Ca^{2+}] accelerated the decay of fluorescence intensity, as shown by the progressive reduction of τ_{avg} to a limiting value of 1.6 ± 0.0027 ns at 35 μM free Ca^{2+} (Fig. 3*A* and supplemental Table S1), indicating a change within the immediate environment of one or more Trp residues.

We found that the Trp fluorescence lifetime of the gating ring was also sensitive to Mg^{2+} (Fig. 3*B*) at concentrations in the millimolar range. As [Mg^{2+}] was incrementally raised from 0 to 12 mM, τ_{avg} progressively decreased to the same limiting value obtained for Ca^{2+} (1.6 ± 0.015 ns; supplemental Tables S1 and S2). Thus, the binding of both Ca^{2+} and Mg^{2+} to the gating ring induced structural transitions at physiologically relevant concentrations, revealing the divalent metal cation-sensing properties of the isolated gating ring apparatus in solution.

The Structural Rearrangements of the Gating Ring Are Ion-specific—The following experiments were designed to estimate the apparent binding constants and assess the specificity of the BK gating ring for divalent cations, based on steady-state fluorescence spectroscopy of intrinsic Trp. The intensity of the fluorescence emission spectra of the gating ring (λ_{ex} = 295 nm) was progressively reduced upon free [Ca^{2+}] elevation in the buffer solution up to 35 μM, as shown in Fig. 4*A*. The [Ca^{2+}]-dependent quenching of the fluorescence intensity at 340 nm was well described by the linear combination of two Hill functions with apparent binding constants $K1_{½}$ = 0.29 ± 0.0043 μM (n_1 = 3.4 ± 0.16) and $K2_{½}$ = 3.5 ± 0.51 μM (n_2 = 2.1 ± 0.35) (Fig. 4*D*), suggesting at least two Ca^{2+}-binding sites and positive cooperativity. This apparent Ca^{2+} affinity is relevant to BK channel activation (4, 54). $K1_{½}$ likely relates to Ca^{2+} binding to the RCK2 domain at the calcium bowl site, whereas the higher $K2_{½}$ value likely reflects Ca^{2+} binding to the RCK1 domain, which has a lower apparent affinity in solution (33, 47), also inferred from electrophysiological investigations (34–37).

The apparent Mg^{2+} affinity, $K_{½}$ = 154 ± 20.7 μM (n = 2.02 ± 0.44) was estimated by fitting to a Hill function the fluorescence intensity at 340 nm acquired at different [Mg^{2+}] (Fig. 4, *B* and *D*). Saturating [Mg^{2+}] produced only an overall ~15% decrease in fluorescence intensity as compared with a 30% reduction observed with saturating [Ca^{2+}].

Previous investigations have shown that Ba^{2+} cannot activate reconstituted BK channels (55, 56); however, excluding Ba^{2+}-dependent BK activation is not trivial due to the blocking action of Ba^{2+} at micromolar concentrations (56) on the internal side of the BK channel selectivity filter (57, 58). We probed whether Ba^{2+} can bind and induce conformational changes to the isolated BK gating ring by measuring intrinsic Trp fluorescence while progressively increasing [Ba^{2+}]. The addition of Ba^{2+} up to 13 mM did not alter the Trp fluorescence intensity of

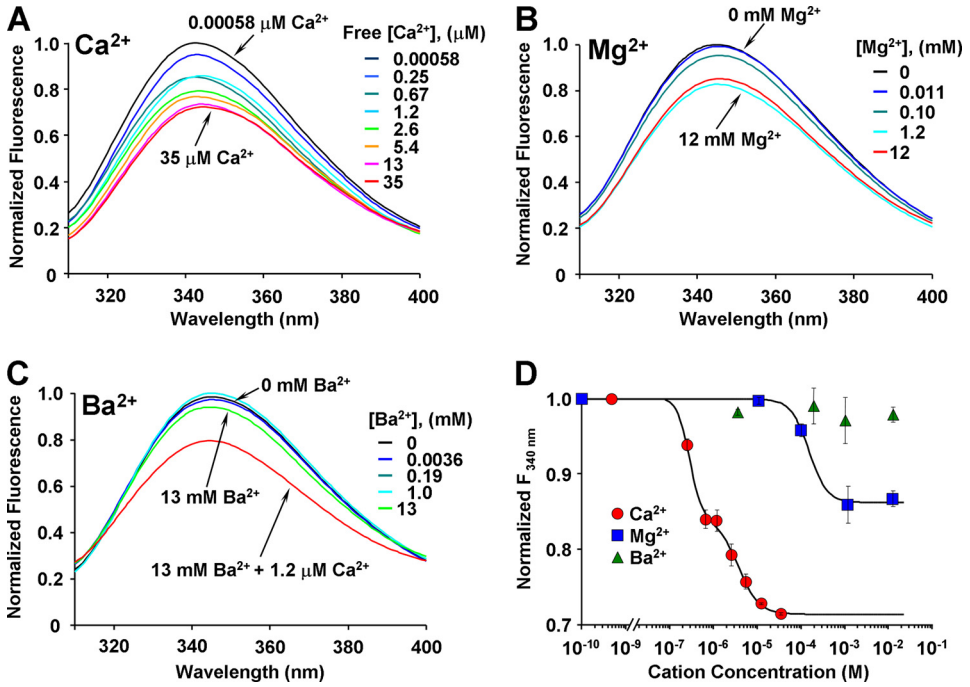

FIGURE 4. **The divalent cation selectivity of the purified BK gating ring.** *A*, normalized representative steady-state emission spectra of the gating ring in solution when excited at 295 nm, acquired under increasing [Ca^{2+}]. Note the dose-dependent quenching effect. *B*, as in *A*, except for increasing [Mg^{2+}] in a nominally Ca^{2+}-free buffer. *C*, as in *B*, except for increasing [Ba^{2+}] up to 13 mM. Note that the lack of Ba^{2+} effects on the gating ring intrinsic Trp fluorescence. After adding Ba^{2+}, the [Ca^{2+}] was increased to 1.2 μM to ascertain gating ring functionality (*red trace*). *D*, the fluorescence intensity (at 340 nm) from experiments as in *A–C* is plotted *versus* the concentration of divalent cations (●, Ca^{2+}; ■, Mg^{2+}; ▲, Ba^{2+}). The experimental points were fit to double (Ca^{2+}) or single (Mg^{2+}) Hill functions. The apparent affinity of the gating ring for Ca^{2+} was: $K1_{1/2} = 0.29 \pm 0.0043$ μM ($n_1 = 3.4 \pm 0.16$) and $K2_{1/2} = 3.5 \pm 0.51$ μM ($n_2 = 2.1 \pm 0.35$), and for Mg^{2+}: $K_{1/2} = 154 \pm 20.7$ μM ($n = 2.02 \pm 0.44$) ($n = 3$).

the gating ring (Fig. 4, *C* and *D*). Nevertheless, when Ca^{2+} was added at the end of the Ba^{2+} experiment, the Trp fluorescence was quenched, confirming that protein activity was intact (Fig. 4*C*, *red trace*). Thus, the isolated gating ring exhibits cationic ligand selectivity, undergoing structural changes upon Ca^{2+} and Mg^{2+} binding with different apparent affinity, whereas not apparently responding to Ba^{2+}.

Effect of Calcium Bowl Neutralization on Divalent Cation Sensitivity—BK channels possess a high-affinity Ca^{2+}-binding site consisting of five consecutive aspartate residues (Asp^{894}–Asp^{898}) called the calcium bowl (29). To investigate the role of the calcium bowl in the sensitivity of the isolated gating ring for cations, we expressed and purified a gating ring carrying the calcium bowl-neutralizing mutations D894A,D895A,D896A, D897A,D898A (supplemental Fig. S3*A*). Calcium bowl neutralization did not seem to alter the overall secondary structure of the gating ring, as suggested by CD spectroscopic analysis (supplemental Fig. S3*B*, supplemental Table S3). However, this gating ring mutant elutes from the size-exclusion column with an apparent molecular mass (>600,000) higher than that of a tetrameric structure. Time-correlated single photon counting revealed that calcium bowl neutralization did not completely abolish the Ca^{2+} sensitivity of the mutant gating ring (Fig. 5*A*) as the average Trp fluorescence lifetime was decreased from $\tau_{avg} = 3.2 \pm 0.015$ ns (0.00058 μM Ca^{2+}) to $\tau_{avg} = 2.7 \pm 0.12$ ns (at 35 μM Ca^{2+}; fitting parameters in supplemental Table S4).

Saturating free [Ca^{2+}] resulted in a significantly smaller degree of steady-state Trp fluorescence quenching in the calcium bowl-neutralized gating ring (~10%; *cf.* WT: ~30% quenching). These data were well fit by a single Hill function, with an apparent Ca^{2+} affinity of 2.0 ± 0.074 μM and a Hill coefficient of $n = 2.4 \pm 0.39$ (Fig. 5, *B* and *D*). This residual Ca^{2+} sensitivity could be due to a high-affinity Ca^{2+}-binding site in RCK1. Interestingly, the calcium bowl mutations completely abolished the gating ring sensitivity for Mg^{2+} (up to 12 mM), suggesting that the Mg^{2+} effects observed for the WT gating ring likely arise from Mg^{2+} binding to the calcium bowl under nominal zero [Ca^{2+}] (Fig. 5, *C* and *D*).

The Apo and Ca^{2+}-bound Conformations of the Gating Ring Have Different Hydrodynamic Radii—The results from fluorescence-based approaches provide evidence for physiologically relevant rearrangements in the BK gating ring induced by cation binding. However, they cannot provide information regarding the extent of the rearrangements involved because Trp fluorophores are reporting changes in their immediate microenvironment. Are these conformational changes associated with a detectable change in the overall gating ring shape? To gain direct insight on the Ca^{2+}-induced conformational transitions, we have analyzed the hydrodynamic properties of gating ring particles in solution using the DLS technique, also known as photon correlation spectroscopy. DLS, which is based on the Brownian motion properties of particles in solution, provides a measurement of the particle hydrodynamic radius (R_H). Rather than a direct measure of particle size, R_H refers to the radius of an ideal hard sphere with the same mass, density, and hydration properties as the investigated protein particles.

Particles with minimal surface-area-to-volume ratio (*i.e.* spheres) with a mass of 312,000 and density and hydration properties relevant to proteins would exhibit a theoretical R_H (R_{H_Theo}) of 5.1 nm. The crystallographically resolved Ca^{2+}-

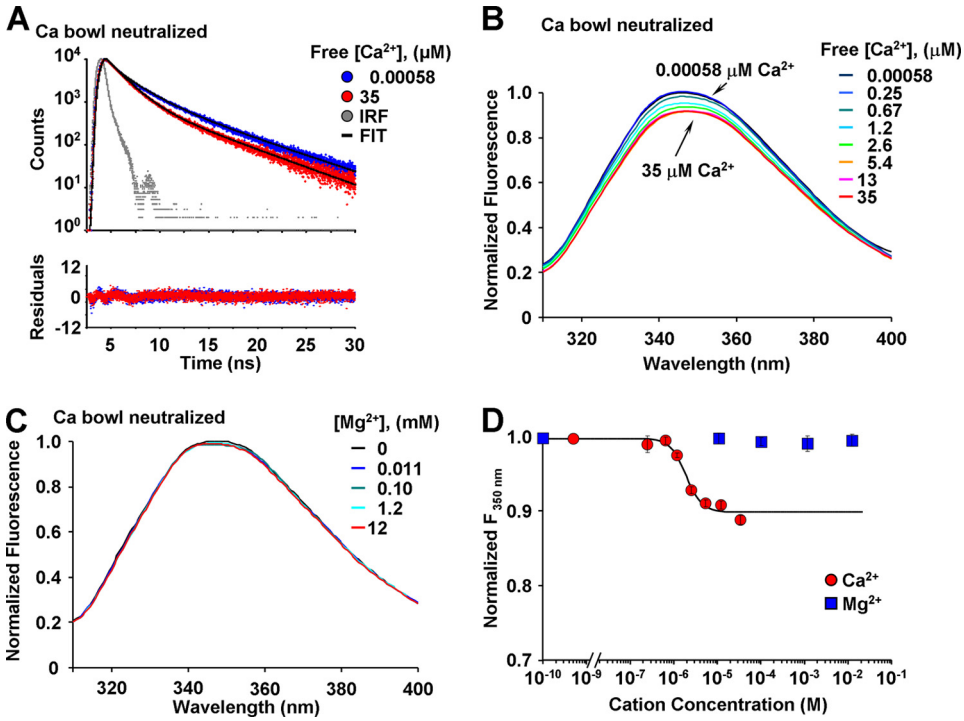

FIGURE 5. **Neutralization of the calcium bowl region reduces the Ca^{2+} sensitivity of the gating ring and abolishes Mg^{2+} sensitivity.** *A*, the intrinsic Trp fluorescence intensity decay of a gating ring carrying the D894A,D895A,D896A,D897A,D898A neutralization within the RCK2 domain, recorded in nominal zero (*blue*) or 35 μM (*red*) free Ca^{2+}. Increasing the [Ca^{2+}] to 35 μM Ca^{2+} produced a modest change in the τ_{avg}, as compared with the wild-type gating ring (Fig. 3*A*). *IRF*, instrument response time. *B* and *C* are fluorescence emission spectra of the calcium bowl mutant gating ring in solution excited at 295 nm. *B*, the Trp fluorescence intensity decreased as the free [Ca^{2+}] of a solution containing the calcium bowl mutant gating ring was increased from nominal zero to 35 μM. *C*, unlike the wild-type gating ring, the calcium bowl mutant did not exhibit Mg^{2+} sensitivity, up to 12 mM. *D*, the fluorescence intensity at 350 nm from experiments in *panels B* and *C* is plotted *versus* the concentration of divalent cations (●, Ca^{2+}; , ■, Mg^{2+}). The experimental points are fit to a Hill function with $K_{1/2} = 2.0 \pm 0.19$ μM and $n = 2.1 \pm 0.35$.

free gating ring (23) has a torus-like shape, with radius ~4.5–6 nm, height ~5 nm, and a 2-nm internal aperture (Fig. 6*A*). As this shape is not spherical, gating ring particles in solution are expected to exhibit a larger R_H than R_{H_Theo}. Indeed, the dominant distribution (71 ± 4.3%) of purified gating ring particles in nominally Ca^{2+}-free solution was estimated to have a mean R_H of 10 ± 0.41 nm (Fig. 6*B*). The particles outside the dominant distribution had $R_H > 60$ nm (most of them around 400 nm) and probably correspond to protein aggregates that were not investigated. The polydispersity of the dominant distribution (*i.e.* the standard deviation divided by mean hydrodynamic diameter) was 12 ± 0.53%, within the range (10–15%) of homogeneous, monodisperse solutions (59).

Notably, when [Ca^{2+}] was elevated to 35 μM, the gating ring R_H was reduced to 7.6 ± 0.14 nm (Fig. 6*B*), which corresponds to a 27 ± 3.5% R_H decrease (Fig. 6*D*). This result suggests that the Ca^{2+}-bound gating ring particles diffuse faster in solution; their shape has less surface-area-to-volume ratio, *i.e.* they are more compact. This Ca^{2+}-induced structural compaction is reversible; decreasing free [Ca^{2+}] from 35 to 0.07 μM by the addition of EGTA almost fully restored the gating ring hydrodynamic radius (9.4 ± 0.47 nm). Mg^{2+} induced a much smaller R_H decrease (7.0 ± 3.5%; Fig. 6, *C* and *D*).

DISCUSSION

Recently resolved atomic structures of the human BK channel intracellular ligand-sensing apparatus have revealed that it is a hetero-octameric assembly of RCK domains (a pair of RCK1 and RCK2 domains from each subunit) arranged to form a gating ring structure (23, 24). This work, which capitalizes on these structural data, is the first attempt to shed light on the molecular mechanisms by which the free energy from ions binding to the human BK channel gating ring structure is transduced into conformational rearrangements required to open the pore. The presumption of this study is that ligands binding to the gating ring induce detectable conformational changes. We have probed for and resolved ligand-induced conformational rearrangements under physiologically relevant conditions. The significant findings of this investigation are as follows. 1) Purified human BK C termini self-assemble under physiologically relevant conditions into tetramers, likely corresponding to gating rings. 2) Ca^{2+} and Mg^{2+} specifically induce conformational changes in the isolated gating ring, whereas Ba^{2+} does not. 3) Neutralization of key residues within the calcium bowl significantly reduces the Ca^{2+} effect on the gating ring rearrangements and eliminates Mg^{2+} sensitivity. 4) Upon Ca^{2+} binding, gating ring particles undergo a fully reversible reduction in their hydrodynamic radii, consistent with a compaction of their structure, whereas Mg^{2+} has a modest effect on the gating ring shape. Crucially, the structural and functional features of gating ring parallel the Ca^{2+}-dependent activation properties of the native BK channel (4, 7, 8, 25, 27, 34, 52, 53).

The Cationic Ligand Selectivity of the Gating Ring—Ca^{2+}, Mg^{2+}, and Ba^{2+} were used to probe the metal-sensing properties of the purified gating ring using its intrinsic Trp fluores-

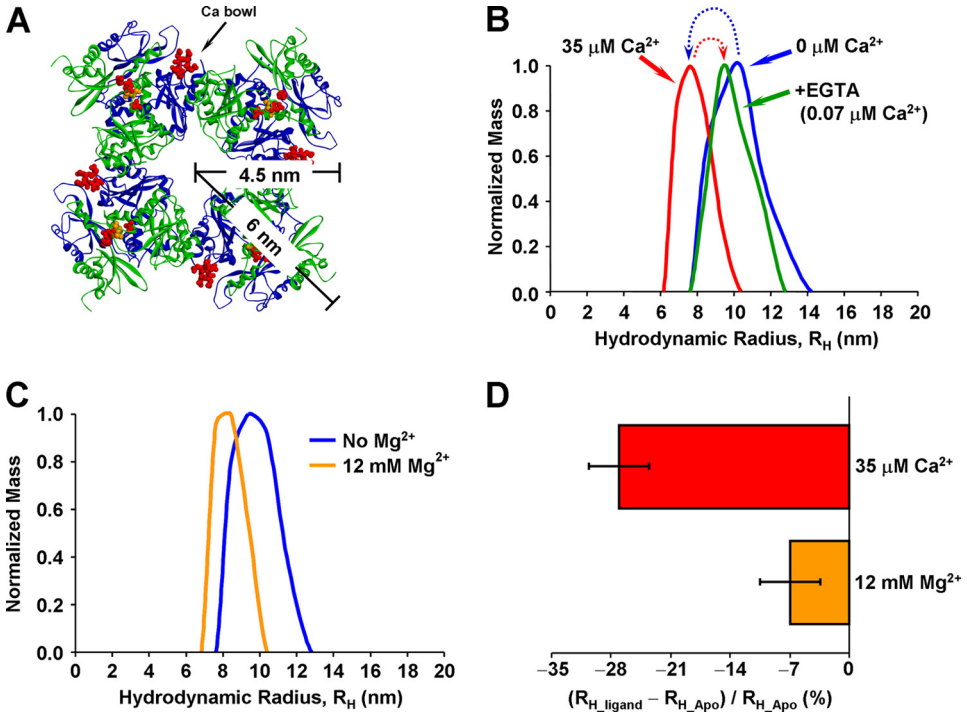

FIGURE 6. **Ca^{2+} reversibly reduces the hydrodynamic radius of the gating ring in solution.** *A*, a top view of the BK gating ring (23), which has a toroidal structure with a diameter ~9–12 nm, a height ~5 nm, and a central aperture of ~2 nm. Residues known to be involved in high-affinity Ca^{2+} sensitivity in the BK gating ring are depicted in *red* (Asp^{362}/Asp^{367} in RCK1 and the calcium bowl in RCK2) or *orange* (Met^{513} in RCK1). *B*, gating ring particle distributions obtained from a characteristic dynamic light scattering experiment. Only the dominant (70%) distributions below 60 nm are shown. The mean R_H of the particle distribution in nominally 0 Ca^{2+} (*blue*) was 10.1 nm. Increasing the free [Ca^{2+}] to 35 μM shifted the distribution toward smaller R_H values, with a mean of 7.8 nm (*red*), consistent with a transition to a more compact conformation. Reducing free Ca^{2+} from 35 to 0.07 μM by the addition of EGTA (*green*) practically restored the original distribution (9.5 nm), demonstrating that the Ca^{2+}-induced rearrangements of the gating ring are reversible. *C*, a characteristic DLS experiment on the gating ring before (R_H = 9.70 nm; *blue*) and after (R_H = 8.65 nm; *orange*) the addition of 12 mM Mg^{2+}. *D*, overall R_H reduction by the addition of saturating ligand concentration to gating ring particles in solution, expressed as the percentile change from the mean ligand-free R_H (R_{H_Apo}). *Error bars* indicate S.E.

cence. Ca^{2+} and Mg^{2+}, known regulators of the BK channel, significantly affected the average lifetime of Trp fluorescence (Fig. 3, *A* and *B* and supplemental Tables S1 and S2), suggesting conformational rearrangements. These results are also supported by steady-state fluorescence measurements, suggesting at least two distinct high-affinity Ca^{2+}-binding sites with $K_{½}$ 0.29 and 3.5 μM (Fig. 4, *A* and *D*), in agreement with the electrophysiologically inferred apparent Ca^{2+} affinity of whole BK channels (4, 34, 35, 37).

The gating ring exhibited significantly less affinity for Mg^{2+} ($K_{½}$ = 154 μM, Fig. 4, *B* and *D*) and was apparently insensitive to Ba^{2+} (Fig. 4, *C* and *D*), defining the cationic ligand selectivity of the BK metal-sensing apparatus. The lack of detectable Ba^{2+}-induced conformational changes is consistent with previous work on reconstituted BK channels that did not show evidence for Ba^{2+}-dependent BK channel activation (55, 56).

However, the well characterized block effect of Ba^{2+} at the BK channel pore (55–58) could confound attempts to characterize an alternative effect of Ba^{2+} on channel activation (56). Because we did not resolve Ba^{2+}-driven conformational changes in the isolated gating ring, we speculate that if Ba^{2+} can activate BK channels, other protein domain(s), in addition to the gating ring, may be required.

How Many High-affinity Ca^{2+}-binding Sites Exist within the Gating Ring?—A recent crystal structure of the BK gating ring in the presence of Ca^{2+} (Protein Data Bank code 3MT5) definitively demonstrated that the calcium bowl region in RCK2 is a Ca^{2+}-binding site (24). This finding was in agreement with previous electrophysiological investigations (29, 34, 35) as well as biochemical investigations of the calcium bowl region (30, 32, 60) and the whole RCK2 domain (33). Although it has yet to be confirmed in atomic structures, electrophysiological investigations support the existence of a second micromolar-affinity Ca^{2+}-bindng site in the RCK1 domain (34–38); indeed, purified RCK1 domains in solution assemble into homo-octameric gating ring-like structures that sense micromolar Ca^{2+} in solution (47).

The Ca^{2+}-induced conformational changes of the purified gating ring detected spectroscopically in this work exhibit a composite Ca^{2+} dependence with $K_{½}$ = 0.29 and 3.5 μM (Fig. 4, *A* and *D*), which implies the existence of more than one type of high-affinity Ca^{2+}-binding site. Furthermore, neutralization of the five consecutive aspartates that comprise the calcium bowl significantly reduced the overall extent of the detectable fluorescence changes (Fig. 5, *B* and *D*) but did not completely eliminate Ca^{2+} sensitivity; calcium bowl gating ring mutants exhibit a single transition with an apparent Ca^{2+} affinity of 2 μM (Fig. 5*D*).

We propose that the transition with higher affinity ($K1_{½}$ = 0.29 μM) is relevant to Ca^{2+} binding to the RCK2 calcium bowl site, whereas the second transition ($K2_{½}$ = 3.5 μM, Fig. 4*D*) arises from Ca^{2+} binding to the RCK1 domain, which has less apparent affinity (34, 35, 37). Supporting this view, the homo-RCK1 gating ring exhibited an apparent Ca^{2+} affinity of 1.7 μM

(47), similar to the lower Ca^{2+} affinity component of the wild-type gating ring (3.5 μM) and the residual Ca^{2+} sensitivity of the calcium bowl mutant (2 μM). Electrophysiological investigations have highlighted residues Asp^{362}, Asp^{367}, Met^{513}, Arg^{514}, and Glu^{535} as candidates for Ca^{2+} coordination in RCK1 (34–38). Consistent with this view, the Ca^{2+} binding properties of isolated RCK1 domains in solution suggest that an RCK1 Ca^{2+}-binding site could exist with multiple Ca^{2+}-coordinating residues (47).

The Calcium Bowl Binds Mg^{2+} with Low Affinity—A low-affinity Mg^{2+}-binding site known to modulate channel activity (61, 62) is likely located at the interface between the RCK1 domains (Glu^{374}, Glu^{399}) and the voltage sensors (Asp^{99}, Asn^{172}) (4, 7, 34, 41–43), enhancing the efficiency of the voltage sensor-gate coupling (63). Because the purified gating ring does not include transmembrane domains, the effects observed in this study (Fig. 4, *B* and *D*) likely arise from Mg^{2+} binding to alternative sites. We found that calcium bowl neutralization completely eliminated the Mg^{2+} effect on the endogenous Trp fluorescence of the gating ring (Fig. 5, *C* and *D*), suggesting that the calcium bowl can bind Mg^{2+} with much less affinity than Ca^{2+}. The addition of Mg^{2+} to the gating ring in the presence of 35 μM free Ca^{2+} induced no further spectroscopically resolvable conformational changes (supplemental Fig. S4), supporting the view that in the isolated gating ring, Mg^{2+} acts through the calcium bowl site as an inefficient Ca^{2+} mimetic, rather than an allosteric ligand. These results recapitulate previous electrophysiological experiments (4, 61, 62, 64), where it was demonstrated that Mg^{2+} competes with Ca^{2+} for the high-affinity Ca^{2+}-binding sites.

The Gating Ring Apparatus Operates as a Selective Chemo-mechanical Transducer of Metal Binding—In this work, we have demonstrated Ca^{2+}-dependent structural rearrangements of the whole human BK channel gating ring apparatus, resolved by the fluorescence emission of native Trp residues and, from a whole-particle perspective, by dynamic light scattering. The latter showed that the gating ring reshapes in response to [Ca^{2+}] binding, toward a "more spherical" or compact conformation characterized by a reduced surface-area-to-volume ratio. As these conformational rearrangements were induced by [Ca^{2+}] relevant to BK channel activation, we propose that they likely constitute the prime molecular events that propagate to the BK channel pore, to increase open probability. In contrast, Mg^{2+} binding produced much smaller changes in the shape of the gating ring (Fig. 6, *C* and D), which suggests that the Mg^{2+}-induced perturbations in the microenvironment of Trp residues (~15% maximal decrease in fluorescence intensity as compared with a 30% reduction observed with saturating [Ca^{2+}]) do not tightly correlate with the global structural rearrangements of the gating ring. Possibly, Trp residues report changes to their microenvironment, which may not reflect the extent of macroscopic structural rearrangements. The binding of Mg^{2+} to the Ca^{2+}-binding sites does not activate the channel (61, 62); therefore, the modest compaction of the gating ring caused by saturating [Mg^{2+}] is likely to be insufficient to facilitate pore opening. Finally, the lack of spectroscopic responses of the gating ring to Ba^{2+} further defined its selectivity for divalent metal cations.

In this work, we probed the divalent metal-sensing properties of the BK channel gating ring under physiological conditions using a combination of spectroscopic (time-resolved and steady-state spectroscopy) and particle-scale (DLS) optical approaches. We have demonstrated that the gating ring responds to elevations in [Ca^{2+}] and, with much less affinity, [Mg^{2+}]. Micromolar Ca^{2+} can induce robust microscopic and macroscopic conformational rearrangements compatible with a compaction of the gating ring superstructure, which likely facilitate pore opening in the whole BK channel. The micromolar sensitivity of the gating ring to Ca^{2+} persists after neutralization of the calcium bowl site, confirming the existence of more high-affinity Ca^{2+}-binding sites. In contrast, millimolar Mg^{2+} can induce changes to a smaller extent than Ca^{2+}, and these changes are probably insufficient to facilitate channel activation *in vivo*. Finally, mirroring the selectivity of the channel to divalent metal agonists, the gating ring underwent no resolvable conformational rearrangements upon [Ba^{2+}] elevation up to millimolar levels. Thus, we have demonstrated that the BK gating ring operates as a selective chemo-mechanical coupler that transduces the free energy of ligand binding into mechanical work that ultimately activates the channel.

Acknowledgments—We thank Debora Nicoll and Tom Vondriska for expert advice and the members of the Olcese laboratory for constructive discussion.

REFERENCES

1. Vergara, C., Latorre, R., Marrion, N. V., and Adelman, J. P. (1998) *Curr. Opin. Neurobiol.* **8,** 321–329
2. Lu, R., Alioua, A., Kumar, Y., Eghbali, M., Stefani, E., and Toro, L. (2006) *J. Physiol* **570,** 65–72
3. Salkoff, L., Butler, A., Ferreira, G., Santi, C., and Wei, A. (2006) *Nat. Rev. Neurosci.* **7,** 921–931
4. Cui, J., Yang, H., and Lee, U. S. (2009) *Cell Mol. Life Sci.* **66,** 852–875
5. Hou, S., Heinemann, S. H., and Hoshi, T. (2009) *Physiology* **24,** 26–35
6. Wu, R. S., and Marx, S. O. (2010) *Kidney Int.* **78,** 963–974
7. Cui, J. (2010) *J. Physiol.* **588,** 4651–4658
8. Latorre, R., Morera, F. J., and Zaelzer, C. (2010) *J. Physiol.* **588,** 3141–3148
9. Latorre, R., and Miller, C. (1983) *J. Membr. Biol.* **71,** 11–30
10. Wallner, M., Meera, P., and Toro, L. (1996) *Proc. Natl. Acad. Sci. U.S.A.* **93,** 14922–14927
11. Meera, P., Wallner, M., Song, M., and Toro, L. (1997) *Proc. Natl. Acad. Sci. U.S.A.* **94,** 14066–14071
12. Stefani, E., Ottolia, M., Noceti, F., Olcese, R., Wallner, M., Latorre, R., and Toro, L. (1997) *Proc. Natl. Acad. Sci. U.S.A.* **94,** 5427–5431
13. Ma, Z., Lou, X. J., and Horrigan, F. T. (2006) *J. Gen. Physiol* **127,** 309–328
14. Savalli, N., Kondratiev, A., Toro, L., and Olcese, R. (2006) *Proc. Natl. Acad. Sci. U.S.A.* **103,** 12619–12624
15. Pantazis, A., Gudzenko, V., Savalli, N., Sigg, D., and Olcese, R. (2010) *Proc. Natl. Acad. Sci. U.S.A.* **107,** 4459–4464
16. Pantazis, A., Kohanteb, A. P., and Olcese, R. (2010) *J. Gen. Physiol* **136,** 645–657
17. Tombola, F., Pathak, M. M., and Isacoff, E. Y. (2006) *Annu. Rev. Cell Dev. Biol.* **22,** 23–52
18. Long, S. B., Tao, X., Campbell, E. B., and MacKinnon, R. (2007) *Nature* **450,** 376–382
19. Bezanilla, F. (2008) *Nat. Rev. Mol. Cell. Biol.* **9,** 323–332
20. Swartz, K. J. (2008) *Nature* **456,** 891–897
21. Fakler, B., and Adelman, J. P. (2008) *Neuron* **59,** 873–881
22. Wang, L., and Sigworth, F. J. (2009) *Nature* **461,** 292–295
23. Wu, Y., Yang, Y., Ye, S., and Jiang, Y. (2010) *Nature* **466,** 393–397

24. Yuan, P., Leonetti, M. D., Pico, A. R., Hsiung, Y., and MacKinnon, R. (2010) *Science* **329,** 182–186
25. Magleby, K. L. (2003) *J. Gen. Physiol* **121,** 81–96
26. Chakrapani, S., and Perozo, E. (2007) *Nat. Struct. Mol. Biol.* **14,** 180–182
27. Lingle, C. J. (2007) *J. Gen. Physiol* **129,** 101–107
28. Ye, S., Li, Y., Chen, L., and Jiang, Y. (2006) *Cell* **126,** 1161–1173
29. Schreiber, M., and Salkoff, L. (1997) *Biophys. J* **73,** 1355–1363
30. Bian, S., Favre, I., and Moczydlowski, E. (2001) *Proc. Natl. Acad. Sci. U.S.A.* **98,** 4776–4781
31. Braun, A. P., and Sy, L. (2001) *J. Physiol.* **533,** 681–695
32. Bao, L., Kaldany, C., Holmstrand, E. C., and Cox, D. H. (2004) *J. Gen. Physiol.* **123,** 475–489
33. Yusifov, T., Savalli, N., Gandhi, C. S., Ottolia, M., and Olcese, R. (2008) *Proc. Natl. Acad. Sci. U.S.A.* **105,** 376–381
34. Xia, X. M., Zeng, X., and Lingle, C. J. (2002) *Nature* **418,** 880–884
35. Bao, L., Rapin, A. M., Holmstrand, E. C., and Cox, D. H. (2002) *J. Gen. Physiol.* **120,** 173–189
36. Zeng, X. H., Xia, X. M., and Lingle, C. J. (2005) *J. Gen. Physiol.* **125,** 273–286
37. Sweet, T. B., and Cox, D. H. (2008) *J. Gen. Physiol.* **132,** 491–505
38. Zhang, G., Huang, S. Y., Yang, J., Shi, J., Yang, X., Moller, A., Zou, X., and Cui, J. (2010) *Proc. Natl. Acad. Sci. U.S.A.* **107,** 18700–18705
39. Yang, J., Krishnamoorthy, G., Saxena, A., Zhang, G., Shi, J., Yang, H., Delaloye, K., Sept, D., and Cui, J. (2010) *Neuron* **66,** 871–883
40. Du, W., Bautista, J. F., Yang, H., Diez-Sampedro, A., You, S. A., Wang, L., Kotagal, P., Lüders, H. O., Shi, J., Cui, J., Richerson, G. B., and Wang, Q. K. (2005) *Nat. Genet.* **37,** 733–738
41. Shi, J., Krishnamoorthy, G., Yang, Y., Hu, L., Chaturvedi, N., Harilal, D., Qin, J., and Cui, J. (2002) *Nature* **418,** 876–880
42. Yang, H., Shi, J., Zhang, G., Yang, J., Delaloye, K., and Cui, J. (2008) *Nat. Struct. Mol. Biol.* **15,** 1152–1159
43. Lee, U. S., and Cui, J. (2010) *Trends Neurosci.* **33,** 415–423
44. Li, M., Tanaka, Y., Alioua, A., Wu, Y., Lu, R., Kundu, P., Sanchez-Pastor, E., Marijic, J., Stefani, E., and Toro, L. (2010) *Proc. Natl. Acad. Sci. U.S.A.* **107,** 19096–19101
45. Hou, S., Xu, R., Heinemann, S. H., and Hoshi, T. (2008) *Nat. Struct. Mol. Biol.* **15,** 403–410
46. Hou, S., Xu, R., Heinemann, S. H., and Hoshi, T. (2008) *Proc. Natl. Acad. Sci. U.S.A.* **105,** 4039–4043
47. Yusifov, T., Javaherian, A. D., Pantazis, A., Gandhi, C. S., and Olcese, R. (2010) *J. Gen. Physiol.* **136,** 189–202
48. Sreerama, N., and Woody, R. W. (2004) *Methods Enzymol.* **383,** 318–351
49. Lakowicz, J. R. (2006) *Principles of Fluorescence Spectroscopy*, 3rd Ed., pp. 97–155, Springer, New York, NY
50. Cantor, C. R., and Schimmel, P. R. (1980) in *Biophysical Chemistry Part II: Techniques for the Study of Biological Structure and Function* (McCombs, L. W., ed) pp. 539–590, W. H. Freeman and Company, New York
51. Jiang, Y., Lee, A., Chen, J., Cadene, M., Chait, B. T., and MacKinnon, R. (2002) *Nature* **417,** 515–522
52. Niu, X., Qian, X., and Magleby, K. L. (2004) *Neuron* **42,** 745–756
53. Qian, X., Niu, X., and Magleby, K. L. (2006) *J. Gen. Physiol.* **128,** 389–404
54. Latorre, R., and Brauchi, S. (2006) *Biol. Res.* **39,** 385–401
55. Vergara, C., and Latorre, R. (1983) *J. Gen. Physiol.* **82,** 543–568
56. Oberhauser, A., Alvarez, O., and Latorre, R. (1988) *J. Gen. Physiol.* **92,** 67–86
57. Vergara, C., Alvarez, O., and Latorre, R. (1999) *J. Gen. Physiol.* **114,** 365–376
58. Carvacho, I., Gonzalez, W., Torres, Y. P., Brauchi, S., Alvarez, O., Gonzalez-Nilo, F. D., and Latorre, R. (2008) *J. Gen. Physiol.* **131,** 147–161
59. Proteau, A., Shi, R., and Cygler, M. (2010) *Curr. Protoc. Protein Sci.* Chapter 17, Unit 17.10
60. Sheng, J. Z., Weljie, A., Sy, L., Ling, S., Vogel, H. J., and Braun, A. P. (2005) *Biophys.J.* **89,** 3079–3092
61. Zhang, X., Solaro, C. R., and Lingle, C. J. (2001) *J. Gen. Physiol.* **118,** 607–636
62. Shi, J., and Cui, J. (2001) *J. Gen. Physiol.* **118,** 589–606
63. Horrigan, F. T., and Hoshi, T. (2008) *Nat. Struct. Mol. Biol.* **15,** 1130–1132
64. Hu, L., Yang, H., Shi, J., and Cui, J. (2006) *J. Gen. Physiol.* **127,** 35–49